MOLEKUL
eISSN: 2503-0310

Articles

https://doi.org/10.20884/1.jm.2024.19.3.11756

Adsorption of Cationic Malachite Green Dye using Easily Separated Adsorbent of Magnetized Coal Fly Ash

Miftakhul Romadhona, Nurul Hidayat Aprilita, Mudasir Mudasir*

Department of Chemistry, Faculty of Mathematics and Natural Sciences, Gadjah Mada University, Sekip Utara Bulaksumur, Yogyakarta 55281, Indonesia

*Corresponding author email: mudasir@ugm.ac.id

Received April 19, 2024; **Accepted** October 24, 2024; **Available online** November 20, 2024

ABSTRACT. A study on the synthesis of magnetized adsorbents from coal fly ash (FA) for the adsorption of malachite green (MG) dye has been conducted. The method involves acid activation and ferrite magnetization of FA. The activation of FA was performed by mixing it in an HCl solution, while the magnetization was carried out by the coprecipitation method using the molar ratio of 1:2 of Fe^{2+}/Fe^{3+}. The magnetized coal fly ash adsorbent (FA/Fe_3O_4) was then utilized to adsorb the MG dye, and the results were compared with that adsorbed by activated fly ash (AFA). Characterization of the materials was carried out using Atomic Absorption Spectroscopy (AAS), Fourier Transform Infrared Spectroscopy (FTIR), X-ray diffraction (XRD), and Vibrating Sample Magnetometer (VSM). The optimized parameters in the adsorption study were pH, adsorbent mass, contact time, and initial concentration. The optimum conditions for the adsorption of MG dye with AFA and FA/Fe_3O_4 are obtained at pH 7, the adsorbent mass of 0.1 and 0.25 g respectively, a contact time of 45 minutes, and the initial concentration of MG dye of 175 ppm. The MG adsorption on both adsorbents follows a pseudo-second-order kinetic model and can be best described by the Langmuir isotherm adsorption model. The synthesized adsorbent is prospective as it is low cost and easily separable from the solution using an external magnet after adsorption.

Keywords: Adsorption, coal fly ash, magnetite, malachite green

INTRODUCTION

Dyes are used in large quantities in many industries including textile, paper, printing, leather, cosmetics, plastic, pharmaceuticals, and food products. The characteristics of their wastewater are deep color and high organic content (Sartape et al., 2017). Waste from synthetic dyes that are directly discharged into the environment will disrupt the lives of organisms and the penetration of sunlight. Synthetic dyes are highly stable against light, difficult to biodegrade, and resistant to aerobic digestion (Kandisa & Saibaba KV, 2016). MG is a cationic dye containing a triphenyl methane group (**Figure 1**) and is widely used as a dye in various industries such as silk, wool, linen, paper, and lather (Mohamed et al., 2019). The presence of the MG dye in high concentrations in water becomes cytotoxic to mammalian cells and can increase tumor growth (Ben et al., 2023). In humans, the MG dye can cause irritation in the respiratory tract and lead to irritation in the digestion tract when ingested. Contact with the skin can result in irritation accompanied by redness and pain. If it comes into contact with the eyes, it can cause permanent eye injury (Chowdhury et al., 2011).

Several methods have been employed to eliminate dyes from wastewater, including oxidation (Islam et al., 2019), coagulation or flocculation (Nourmoradi et al., 2016), membrane technology (Lee et al., 2016), and ion exchange (Yagub et al., 2014). The methods have disadvantages such as using chemicals in large quantities, producing amounts of sludge, high operational costs, long reaction times, and do not exhibit significant effectiveness (Umaningrum et al., 2023). One of the alternative methods for effective wastewater treatment is adsorption. Several types of adsorbents have been widely used, such as silica gel (Sulistiyo et al., 2020), biofilm (Zhang et al., 2022), polystyrene resin (Zhang et al., 2014), magnetic nanoparticles (Du et al., 2022), active carbon (Jeyaseelan et al., 2023), chitosan -zeolite (Kazemi & Javanbakht, 2020), and fly ash (Bharath Balji et al., 2022). An adsorbent is considered to be a good one if it is readily available in nature, simple process, cost-effective, easily regenerated, and eco-friendly (Karanac et al., 2018).

Coal fly ash (FA) is a solid waste generated from the combustion of coal, consisting of fine particles carried by exhaust gases and captured by an electric precipitator. As a solid waste, FA is relatively cheap compared to other materials such as zeolite, silica gel, or commercial clay. Moreover, it is mostly abandoned near the plants which can potentially be dangerous to the environment. The main chemical constituents of FA

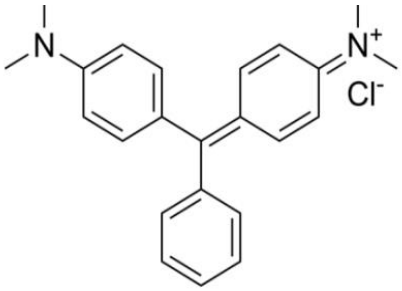

Figure 1. Chemical structure of malachite green

are silica (SiO_2) and alumina (Al_2O_3). Therefore, it has a large surface area and provides active charged sites, making it highly potential to be used as an adsorbent (Saakshy et al., 2016).

There are several modifications to FA as an adsorbent such as activation and magnetization (Bojinova & Teodosieva, 2016; Harja et al., 2021). The activation process can reduce the mineral impurities to increase the active sites of SiO_2 and Al_2O_3 (Valeev et al., 2018). Magnetic modification on the surface of FA is carried out by contacting it with Fe_3O_4 through the coprecipitation method. Magnetization of the FA aims to induce magnetic properties, thus facilitating the simple separation between adsorbent and adsorbate using an external magnet after the adsorption process.

Therefore, in this study, we have investigated the adsorption of the MG dye using magnetic adsorbents prepared from FA. Through this research, it has been successfully determined the adsorption parameters such as MG adsorption, kinetic study as well as its isotherm adsorption. The MG adsorption parameters have been obtained by optimal conditions of solution pH, adsorbent mass, contact time, and initial dye concentration.

EXPERIMENTAL SECTION

Materials

The materials used in this research have analytical grade quality from Merck, including MG dye, hydrochloric acid (HCl), fluoric acid (HF), distilled water, double-distilled water, ammonia (NH_4OH), Iron (III) chloride hexahydrate ($FeCl_3.6H_2O$), iron (II) Sulfate Heptahydrate ($FeSO_4.7H_2O$), and sodium hydroxide (NaOH). Other materials used in this study are whatman-42 filter paper, universal pH indicator paper, and fly ash from the Cilacap power plant.

Instrumentation

The equipment used in this research includes Pyrex laboratory glassware (beakers, glass funnels, volumetric flasks, watch glasses, measuring pipettes), a set of reflux apparatus, a magnetic stirrer, an analytical balance (Mettler AE 200), and a pH meter (YY-400 4in1) along with universal pH indicator. Instruments utilized for the analysis and characterization of coal fly ash include UV-Vis Spectrophotometer (HANNA-Iris H11801), XRD (Philips XRD X'Pert MS), FTIR (8201 PC Shimadzu), AAS (GBS AA atomic absorption spectrophotometer), and VSM (VSM 250).

Preparation of Coal Fly Ash

Coal fly ash from PLTU (electricity power plant), Cilacap, Central Java, Indonesia as much as 25 g was sieved through a 250-mesh sieve and then washed with distilled water until the water showed a neutral pH. The fly ash was filtered and heated in an oven at 100°C until dry. The dried fly ash (FA) was then characterized using FTIR, XRD, and AAS instruments.

Activation of Coal Fly Ash

FA was activated by doing the reflux of 10 g of FA with 600 mL of HCl 6 M solution for 4 hours at 100°C. The activated fly ash (AFA) was washed with distilled water until the filtrate reached a neutral pH, it was then filtered and dried in an oven at 100°C for 6 hours. The obtained solid AFA was characterized by FTIR, XRD, and AAS.

Determination of Point of Zero Charge (PZC) of Magnetized Coal Fly Ash

A total of 40 mL of 0.01 M NaCl solution was adjusted to various pH of 2, 3, 4, 5, 6, 7, 8, 9, 10, and 11 with 0.1 M NaOH or 0.1 M HCl. A total of 0.2 g of magnetized fly ash was then added to the pH-adjusted NaCl solution, shaken for 2 hours, and left overnight. The mixture solution was then filtered, and the final pH was measured. Furthermore, a graph was made between ΔpH (the differences of initial and final pH values) and the initial pH value. The PZC value of the material was obtained from the initial pH value when ΔpH passed the zero point.

Synthesis of Magnetized Fly Ash

The solid AFA (2 g) was added to a 100 mL solution containing $FeCl_3.6H_2O$ and $FeSO_4.7H_2O$ with concentrations of 0.0025 M and 0.0125 M respectively and stirred for 1 hour. The mixture of AFA and Fe^{2+}/Fe^{3+} solution was stirred continuously until the homogeneous solution was attained and then heated to a temperature of 85°C. A solution of NH_4OH (5 M) was added dropwise to the mixture until it reached a pH of 11. the mixture was stirred for 1 hour, and once the temperature dropped, the mixture was filtered and washed using deionized water until it reached a neutral pH. The obtained solid was then dried in an oven at 100°C for 1 hour. Subsequently, it was characterized using FTIR, XRD, and VSM instruments.

Optimization Conditions for Removal of MG Dye

Effect of Solution pH

MG solution with a volume of 20 mL and concentration of 50 ppm was adjusted to pH 3, 4, 5, 6, 7, and 8. Each solution was then added with 0.05 g of magnetized FA and subjected to the adsorption process for 60 minutes. After the adsorption process was completed, the adsorbent was separated using a neodymium magnet, and the obtained filtrate was analyzed by a UV-Vis spectrophotometer. The calibration graph for the determination of MG concentration was made in the range of 0.0-10.0 mg/L by dissolving MG dye in double distilled water and diluting it as required. The absorbance of the solution was then measured by UV-Vis Spectrophotometry at the maximum wavelength (λ_{max}) of 618 nm. The same procedure was also carried out using AFA as an adsorbent, but the adsorbent was filtered through the Whatman filter paper after adsorption. A control solution for every pH was also prepared with a similar procedure but without the addition of adsorbent. The percentage of MG removal (*Re*%) was calculated based on equation (1).

$$Re\% = \frac{(C_o - C_e) * 100\%}{C_o} \quad (1)$$

Where C_o and C_e are the concentrations of initial (before) and final (equilibrium) adsorption of the dye solution.

Effect of adsorbent mass

The MG dye solution, each with a concentration of 50 ppm, was adjusted to their optimum pH value of the adsorption. Magnetized fly ash adsorbent was then added to each dye solution with varying masses of 0.005, 0.100, 0.150, 0.200, 0.250, 0.300, 0.350, and 0.400 g. The mixture solution was stirred for 60 minutes to allow the equilibrium adsorption of MG. After adsorption completion, the adsorbent was separated using a neodymium magnet, and the obtained filtrate was analyzed by a UV-Vis Spectrophotometer at the corresponding maximum wavelength for the dye. The same procedure was also carried out for the AFA adsorbent, but the adsorbent was filtered through the Whatman filter paper after the adsorption process. The control solution was prepared by the same procedure but without the addition of the adsorbents.

Effect of interaction time

The solution of MG dye with a concentration of 50 ppm in 20 mL, was adjusted to their optimum pH and adsorbent mass. The interaction time of MG adsorption varied from 5, 15, 45, 60, 75, and 90 minutes. After completion of the adsorption process, the adsorbent was separated using a neodymium magnet, and the obtained filtrate was subsequently analyzed by a UV-Vis spectrophotometer at the respective maximum wavelength. The same procedure was also carried out for AFA adsorbent, but the adsorbent was filtered through the Whatman filter paper. The control solution for every interaction time was prepared by the same procedure but without the addition of adsorbent.

The adsorption kinetics model was determined from experimental data obtained from this experiment and evaluated by pseudo-first-order as given in Equation (2) (Lagergren, 1898).

$$\ln(q_e - q_t) = \ln q_e - k_1 t \quad (2)$$

where q_e (mg g^{-1}) is the adsorption capacity at equilibrium and q_t (mg g^{-1}) is the adsorption capacity at a certain time t; k_1 is the rate constant of the pseudo-first-order (min^{-1}) model. Plotting of ln ($q_e - q_t$) versus *t*, the values of k_1 and q_e can be calculated from the slope and intercept, respectively. For the kinetic model of pseudo-second order, it was evaluated by equation (3).

$$\frac{t}{q_t} = \frac{1}{k_2 q_e^2} + \frac{1}{q_e} t \quad (3)$$

Plotting the value of t/q_t against *t* gave a slope value of $1/q_e$ and an intercept of $1/k_2 q_e^2$, and both q_e and k_2 (rate constant of pseudo-second order) values can then be calculated from the values of the slope and intercept, respectively.

Effect of initial concentration of MG dye

The solution of MG dye, with varying concentrations of 15, 25, 50, 75, 100, 125, 150, 165, 175, 185, and 200 ppm, each in 20 mL, was adjusted to their optimum pH and mass of adsorbent. The adsorption process for each solution was conducted in accordance with the optimum contact time. After the adsorption process was completed, the adsorbate was separated using a neodymium magnet, and the obtained filtrate was then analyzed using a UV-Vis spectrophotometer. The same procedure was also carried out for the AFA adsorbent, but the adsorbent was filtered through the Whatman filter paper after the adsorption. The control solution for each initial concentration of MG was treated by the same procedure but without the addition of the adsorbent.

Adsorption isotherms were studied using the Langmuir in Equation (4) (Mourabet et al., 2011) and Freundlich isotherm in Eq. (5) (Tighadouini et al., 2019) models by analyzing the adsorption data of MG dye carried out at various concentrations.

$$\frac{C_e}{q_e} = \frac{C_e}{q_m} + \frac{1}{q_m K_L} \quad (4)$$

The q_m (maximum capacity) and K_L (Langmuir constant) values were obtained from the slope and intercept on the linear plot between C_e/q_e against C_e.

$$log q_e = log K_F + \frac{1}{n} log C_e \quad (5)$$

The K_F (Freundlich constant and *n* values were calculated from the intercept and slope of the log q_e *versus* log C_e, respectively.

If the adsorption follow the Langmuir model, the adsorption energy (E_{ads} in kJ mol^{-1}) can be calculated from standard Gibbs energy (ΔG) relation using the value of K_L where E_{ads} is equal to positive sign of Gibbs energy as given in Equation (6).

$$E_{ads} = -\Delta G = RT \ln K_L \quad (6)$$

RESULTS AND DISCUSSION

AAS Characterization

Determination of FA and AFA compositions has been performed to know the effectiveness of the acid activation in removing impurities available in FA by comparing their composition before and after activation. The analytical results of component content in FA and AFA determined by AAS are shown in **Table 1**.

Based on the analytical results as collected in **Table 1**, it is shown that the main minerals contained in FA are SiO_2 and Al_2O_3. Undesirable metal oxides present in FA that will be used as an adsorbent are MgO, Fe_2O_3, and CaO, hereafter referred to as impurities. The decrease in the impurity content on AFA is due to the capability of these metal oxides to dissolve in acid during the activation process except SiO_2. As a result, the relative content of SiO_2 in AFA increases, while the content of other oxides decreases including Al_2O_3. The slight decrease in Al_2O_3 is probably due to partial dealumination processes during acid activation (Muttaqii et al., 2019).

FTIR Characterization

To identify the functional groups of material adsorbents, characterization using FTIR has been conducted and the FTIR spectral profiles for FA, AFA, Fe_3O_4, and Fly Ash/Fe_3O_4 (FA/Fe_3O_4) are shown in **Figure 2**. AFA experienced slight shifts in its absorption peaks compared to its original material FA. There was a broad absorption at the wavenumber of 3449 cm^{-1} in both FA and AFA, indicating the stretching vibration of O—H in the silanol (Si—OH), aluminol (Al—OH) groups, and water molecules absorbed by the materials. This absorption was further supported by the presence of binding vibrations of the —OH group at wavenumbers 1628 cm^{-1} for FA and 1636 cm^{-1} for AFA. The shift in the peak of the asymmetric stretching vibration of Si—O from 1080 cm^{-1} (FA) to 1096 cm^{-1} (AFA), with a sharper peak in AFA, suggests the existence of a stronger Si—O stretching vibration. The presence of peaks at 471 cm^{-1} in FA and 462 cm^{-1} in AFA indicates the bending vibration of Si—O—Si in coal fly ash and bottom ash (FABA) (Huda, et al, 2023). These peaks experienced a shift and became sharper in the AFA, providing clearer confirmation that the AFA has lower impurities and thus has been successfully activated (Nikmah, et al, 2023).

Table 1. The metal oxide content in coal fly ash (FA) and activated fly ash (AFA)

Metal oxides	Content (%, b/b)	
	FA	AFA
SiO_2	71.06	74.55
Al_2O_3	15.19	14.29
MgO	6.28	3.69
Fe_2O_3	3.87	2.76
CaO	3.63	2.92

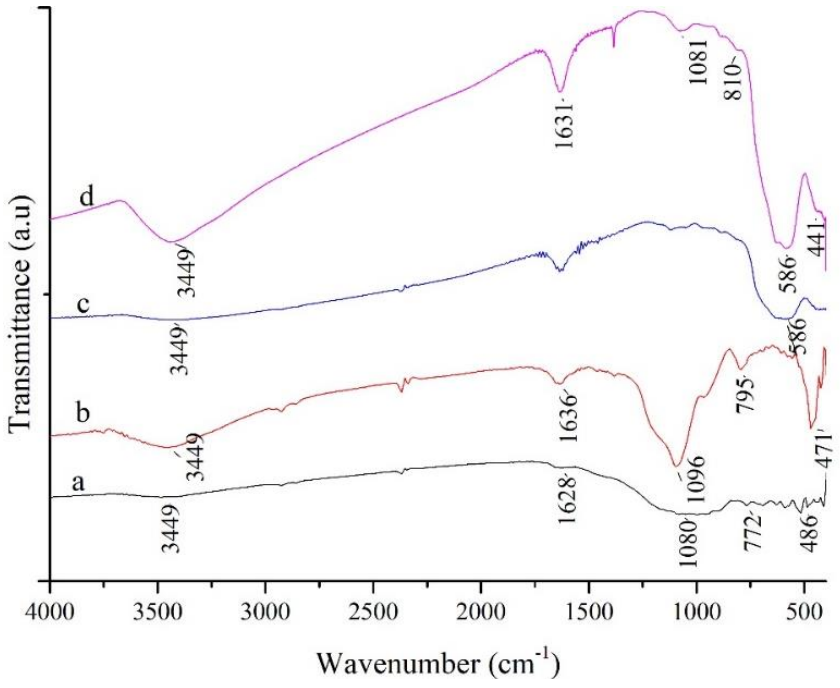

Figure 2. FTIR spectra of FA (**a**), AFA (**b**), Fe_3O_4 (**c**), FA/Fe_3O_4 (**d**).

Based on the spectral profiles of FTIR as shown in **Figure 2**, the broad and intense absorption at the wavenumber of 3449 cm^{-1} in AFA and FA/Fe_3O_4 indicates the stretching vibration of O—H bonds from water molecules. The overlapping peak forms hydrogen bonds with the stretching vibration of O—H from silanol groups on the surface of fly ash. The peak at the wavenumber of 1628 cm^{-1} in AFA shifts to 1631 cm^{-1} in FA/Fe_3O_4, suggesting the presence of bending vibration of O—H from Si—OH or Al—OH groups (Mesdaghinia et al., 2017).

Vibrations of asymmetric stretching of O—Si—O or O—Al—O appear at the wavenumber of 1096 cm^{-1} in AFA, shifting to 1081 cm^{-1} in FA/Fe_3O_4, and the peak width is narrower than AFA (Susiana, et al, 2024). This shift is due to the addition of iron (Fe) species from the magnetic component on the surface of fly ash. The O—Si—O stretching vibration at 795 cm^{-1} in AFA shifts to 810 cm^{-1} in FA/Fe_3O_4, and adsorption also appears in AFA at the wavenumber of 471 cm^{-1}, shifting to 441 cm^{-1} in FA/Fe_3O_4. This indicates the presence of Si—O—Si bending vibrations (Huda, et al, 2023).

The characteristic absorptions of Fe_3O_4 are present at the wavenumbers of 3449 cm^{-1} and 586 cm^{-1}. The absorption at the wavenumber of 3449 cm^{-1} indicates the stretching vibration of O—H from water or Fe—OH groups, while the wavenumber of 586 cm^{-1} indicates the vibration of Fe—O in magnetite (Susiana, et al, 2024). The wavenumber of 586 cm^{-1} also appears in FA/Fe_3O_4. The position of this spectral peak is like that present in Fe_3O_4, proving that the vibration of the Fe—O bond is available in FA/Fe_3O_4. Therefore, it has been confirmed that AFA has been successfully magnetized with ferrite to yield FA/Fe_3O_4 (Suyanta, et al, 2022).

XRD Characterization

Based on the COD diffractogram data, peaks appearing at 2θ 20.79; 26.57; 36.42; 39.37; 40.16; 42.31; 59.75; 67.95 (COD 00-900-5019) correspond to quartz (SiO_2), while peaks appearing at 2θ 23.38; 25.83; 27.81; 30.82; 33.24; 34.50; 35.49; 42.92; 54.71; 57.11; 60.73 (COD 00-210-8043) correspond to mullite ($Al_6Si_2O_{13}$). The obtained data indicate that both quartz and mullite minerals are present in both FA and AFA. Quartz dominates and exhibits higher intensity compared to mullite, thereby indicating that the main component with the highest crystallinity present in AFA is quartz. The results have shown a decrease in crystal intensity and growth, which could represent the crystallinity characteristics of fly ash. The higher the peak intensity in the diffractogram, the higher the crystallinity. In FA, there are still small peaks visible, which are impurities present in the FA, whereas, in AFA, these impurities have decreased due to the acid activation process (Jumaeri W et al., 2007).

Based on **Figure 3**, it is evident that characteristic diffraction peaks appear in the 2θ range of 30.20; 35.59; 43.28; 53.75; 57.22; 62,85 represent the diffraction pattern of Fe_3O_4 particles. These characteristic peaks align with the data recorded in COD 00-153-2800 at a 2θ value of 30.15; 35.51; 43.33; 53.71; 57.06; and 62.86, which specifically refers to magnetite. The FA/Fe_3O_4 adsorbent exhibits peaks similar to those of activated fly ash and Fe_3O_4, but its intensity is decreased. The peaks of the Fe_3O_4 diffractogram in the FA/Fe_3O_4 adsorbent appear to have a slightly reduced intensity compared to pure Fe_3O_4. This decrease is due to a reduction in the crystallinity of Fe_3O_4 within the FA/Fe_3O_4 adsorbent. The decrease in intensity suggests there is an interaction occurring between the surface of the fly ash and Fe_3O_4 within the FA/Fe_3O_4 adsorbent. Based on the characterization results using XRD, it can be concluded that the AFA has successfully been modified with Fe_3O_4 (Gracias, et al, 2022).

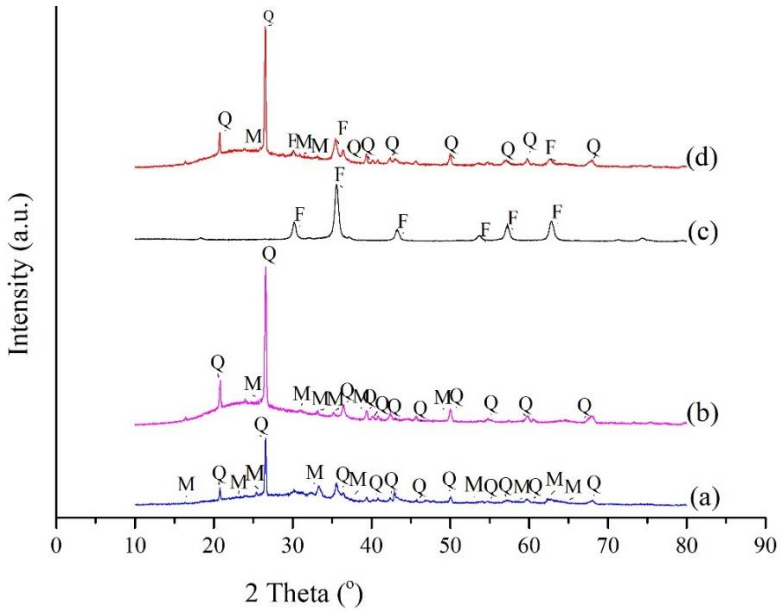

Figure 3. XRD patterns of FA (**a**), AFA (**b**), Fe_3O_4 (**c**), and FA/Fe_3O_4 (**d**) (Q = Quartz, M = Mullite, F = Fe_3O_4)

VSM Characterization of FA/Fe_3O_4

The analysis to measure the magnetic properties of modified materials involves the use of a VSM. The results of magnetic analysis of ferrite and magnetized AFA (FA/Fe_3O_4) using VSM are given in **Figure 4**. The control material of Fe_3O_4 and the synthesized FA/ Fe_3O_4 are classified as soft magnetic materials. Observing the hysteresis curve, it demonstrates a nearly symmetric loop when subjected to the magnetic field and when the magnetic field is removed. Additionally, the narrow area of the hysteresis curve indicates that magnetization requires very little energy.

The hysteresis curve provides information about M_s (magnetic saturation) for each material. M_s indicates the saturation point of a material when subjected to an external magnetic field. Increasing the strength of the applied magnetic field on a material leads to a change in the magnetic moment until it reaches saturation. According to Rosiati (2016), the magnetic strength of magnetite (Fe_3O_4) is significantly greater than that of magnetite composite.

The sample has a M_s value of 8.3 emu/g. When an external magnetic field is applied, with an H value at 0.002 T, the magnetization remnant (M_r) of the sample is 1.14 emu/g. Meanwhile, the coercivity value (H_c) for a sample is 0.011 T. Based on the values of M_s, M_r, and H_c, it can be concluded that the sample belongs to superparamagnetic materials, meaning that it will attain saturation magnetization when subjected to a high magnetic field. A coercivity value (H_c) which is smaller than 0.03 T indicates that the material can be categorized as soft magnetic materials.

The value of M_s in the control is greater than that of FA/Fe_3O_4, indicating that a composite with another material can affect the magnetic properties of pure Fe_3O_4. The possibility here is that when magnetite is composited into fly ash, it may cover the surface of Fe_3O_4, thereby obstructing the active sites of Fe_3O_4. Consequently, FA/Fe_3O_4 has a low magnetic susceptibility, yet it can still be attracted by an external magnetic field and is easily separated from a solution.

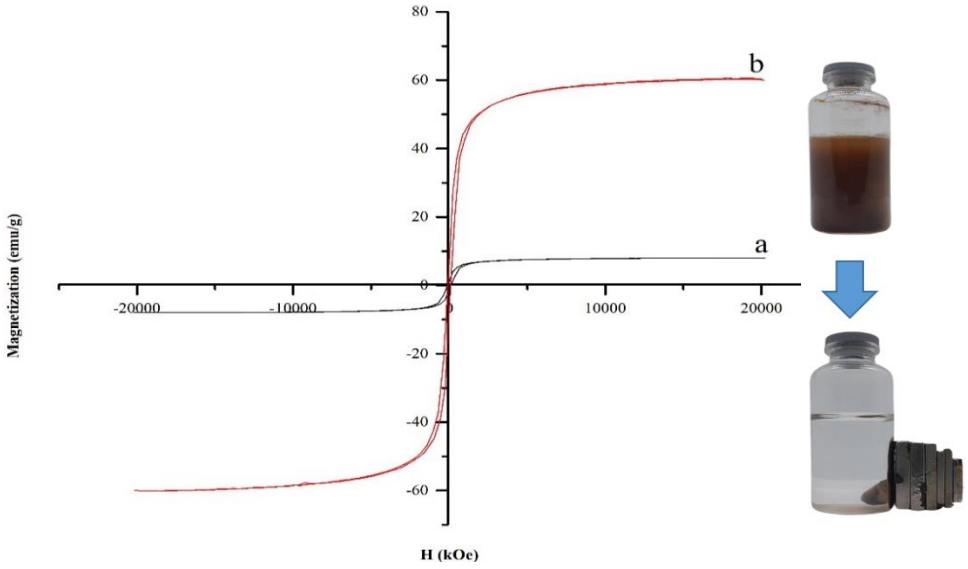

Figure 4. VSM magnetization curves of FA/Fe_3O_4 (**a**) and Fe_3O_4 (**b**). Insert: illustration of easily recoverable adsorbent after application.

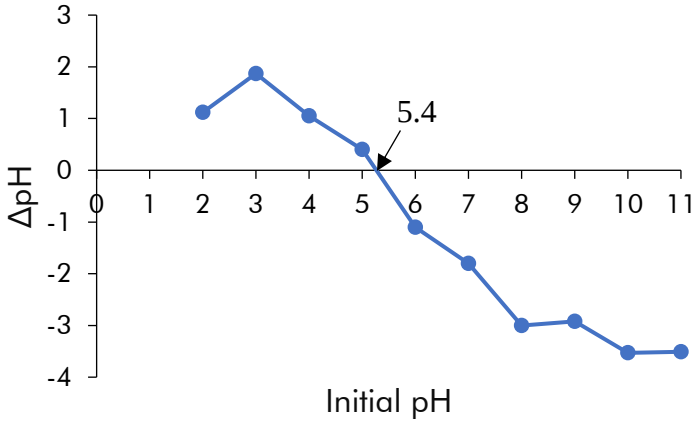

Figure 5. The Point of zero charge (PZC) of FA/Fe_3O_4.

Point of Zero Charge (PZC)

PZC is the state of a material when its surface is neutrally charged. Determining the PZC of a material is crucial to understanding its surface properties in water as it plays a role in being a coating material. Furthermore, this knowledge is important in the wastewater treatment process. The result of PZC determination of FA/Fe_3O_4 can be seen in **Figure 5**.

The result of the plot between ΔpH and initial pH (**Figure 5**) indicates that the ΔpH that equals zero occurs at an initial pH of 5.4, indicating that the point of zero charge (PZC) for FA/Fe_3O_4 is at pH = 5.4. When the solution pH is below this PZC value, the adsorbent surface is predominantly positively charged. Meanwhile, when the solution pH is above the PZC, the adsorbent surface is dominated by a negative charge which is suitable for absorbing the positively charged species such as cationic dyes.

Adsorption Study

Effect of solution pH

The influence of pH on the adsorption of MG dye by FA/Fe_3O_4 adsorbent has been systematically studied. The dye adsorption usually has different optimal pH because pH affects the surface charge of the adsorbent and the charge of the dye. The MG adsorption results on FA/Fe_3O_4 at various pH are shown in **Figure 6**.

The highest percentage of MG adsorption occurs at pH 7 for both AFA and FA/Fe_3O_4. At lower pH (pH<7), there is a low percentage of adsorption due to an abundance of H^+ ions, causing the surface of the adsorbent to be protonated to yield a positively charged surface, which hinders the adsorption of cationic MG dye. This positive charge of the surface repels and reduces its interaction with the cationic dye of MG, thus lowering the percentage of MG adsorption at acidic pH levels. The optimum adsorption of MG dye occurs at pH 7, which is similar to the pH that has been previously reported for the optimum pH of MG adsorption with biogenetic silica nanofiber composites (Mohamed et al., 2019).

After reaching the optimum pH, the percentage of MG adsorption decreases with the increase in the pH of the solution, due to the higher concentration of OH^- ions. These ions induce competition with the negatively charged surfaces of the adsorbent. The OH^- ions interact with the positive charge of the cationic MG dye, forming neutral species that are difficult to adsorb onto the negatively charged surface of the adsorbent. Consequently, the adsorption process between the MG dye and adsorbent, either on AFA or FA/Fe_3O_4, becomes unfavorable, leading to a decrease in the percentage of adsorption as the pH increases. Results of our study show that the percentages of MG adsorption for AFA and FA/Fe_3O_4 adsorbents are 77% and 85%, respectively. It is seen that the percentage of MG adsorption using FA/Fe_3O_4 is larger than that of AFA. This is probably due to the significant role of more diverse active sites available on FA/Fe_3O_4 that include SiO^-, AlO^-, and FeO^- active sites (Susiana, et al, 2024; Gracias, et al, 2022; Suyanta et al., 2022).

Effect of adsorbent mass

The study of the adsorbent mass influence on the effectiveness of the adsorption aims to determine the minimum required mass for the efficient adsorption of dyes. The study has been conducted under the optimum condition of pH obtained from the previous experiment, e.g. pH 7. The adsorbent mass of AFA has been varied in the range of 0.0005 to 0.4 g, while for FA/Fe_3O_4, it is in the range of 0.001 to 0.25 g. The adsorption contact time is kept constant at 60 minutes. The results of the MG adsorption at various adsorbent masses are presented in **Figure 7**.

The adsorption of MG dye using AFA and FA/Fe_3O_4 adsorbent achieves their maximum percentages at the adsorbent masses of 0.25 g and 0.1 g for AFA and FA/Fe_3O_4 adsorbent, respectively. This optimum mass condition can be interpreted as a state where the adsorbent efficiently absorbs the 20 mL MG dye with a concentration of 50 ppm. At each optimum adsorbent mass, AFA can adsorb the MG dye up to 86%, whereas FA/Fe_3O_4 can adsorb the MG dye up to 95% probably due to the additional active sites of FeO^- from magnetite. Again, these results suggest that the FA/Fe_3O_4 adsorbent is more efficient in adsorbing the MG dye because with a smaller amount of adsorbent mass, it can absorb the MG dye at a higher percentage of adsorption.

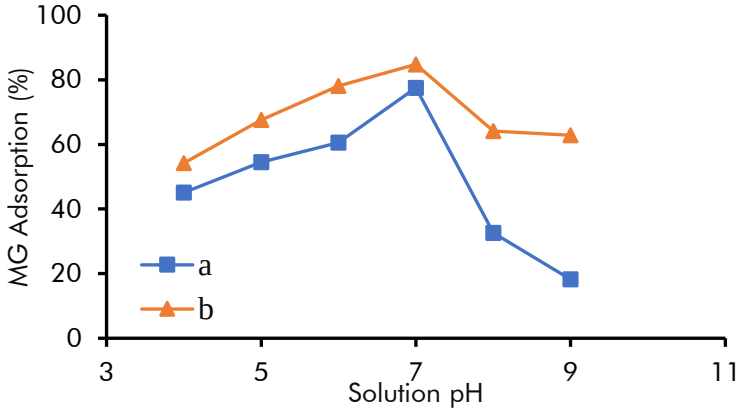

Figure 6. Effect of pH on the adsorption of MG on AFA (a) and FA/Fe_3O_4 adsorbents (b).

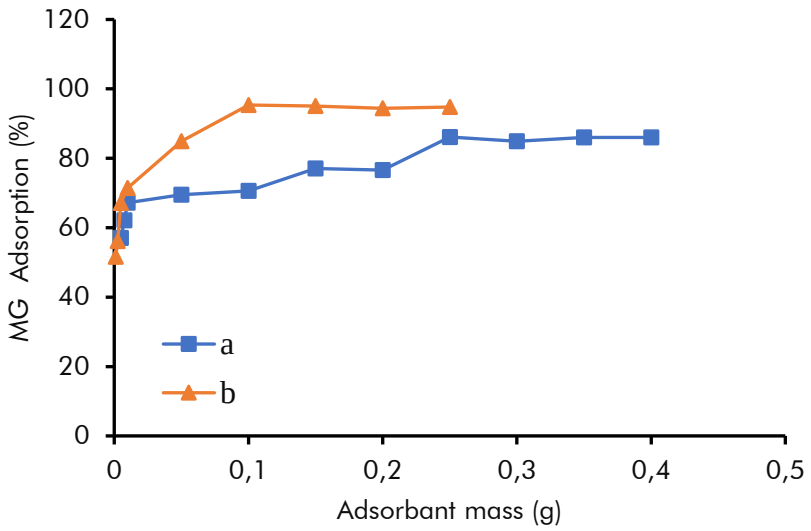

Figure 7. Effect of adsorbent mass on the adsorption of MG dye on AFA (a) and FA/Fe_3O_4 adsorbents (b).

Effect of contact time and kinetics studies

The data obtained from the study about the effect of contact time on the adsorption capacity of MG dye can be seen in **Figure 8**. The optimum contact time for MG adsorption on AFA and FA/Fe_3O_4 adsorbents is 45 minutes. The MG adsorption capacities for AFA and FA/Fe_3O_4 adsorbents at the optimum contact time are 3.69 and 8.54 mg/g, respectively.

The adsorption capacity increases with an increase in contact time. This can be associated with the increase in the probability of occurring interactions between the adsorbate and adsorbent. The length of contact time influences the interaction probability between adsorbent and adsorbate. The longer the contact time, the greater the opportunity for adsorbate to interact with the active sites present on the surface of the adsorbent. As a result, the amount of dye absorbed also becomes larger. After reaching the optimum conditions, the adsorption capacities of dyes for both adsorbents experience a slight decrease. This decrease in adsorption capacity is possibly caused by the desorption process of the dyes that have been absorbed by the adsorbent due to the continuous adsorption processes that are accompanied by stirring. The continuous agitation after the equilibrium state may result in some of the previously absorbed dyes being released back, thus slightly reducing the adsorption capacity.

Determination of the adsorption kinetics model in the adsorption process is often done by comparing the coefficient of the determination (R^2) values from each adsorption kinetics model. A value of R^2 approaching 1 for a certain kinetics model indicates the best model in the adsorption process. In this study, the evaluation of the adsorption kinetics model for the adsorption of MG dye using AFA and FA/Fe_3O_4 adsorbents has been performed with pseudo-first-order and pseudo-second-order kinetics models, and the results of the evaluation are collected in **Table 2**.

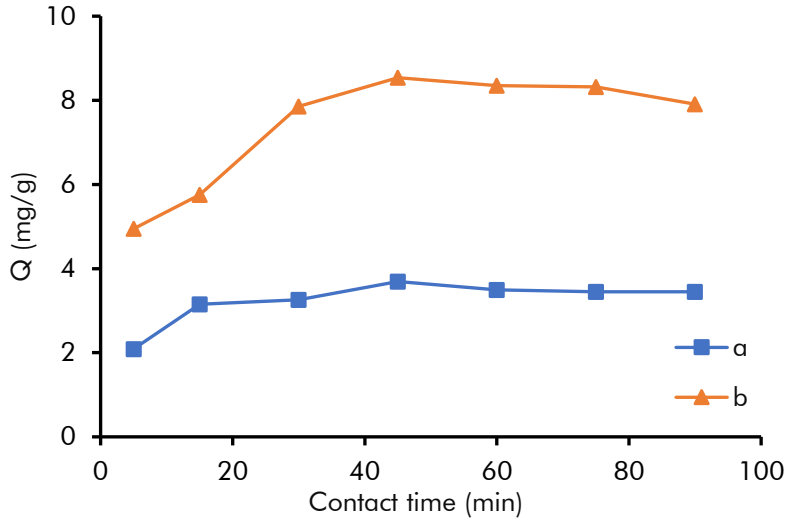

Figure 8. Effect of contact time on MG adsorption capacities (Q) for AFA (a) and FA/Fe_3O_4 (b) adsorbents.

Table 2. Evaluation of the adsorption kinetics model of MG on AFA and FA/Fe_3O_4

Sample	Pseudo-first order		Pseudo-second order	
	k_1 (min^{-1})	R^2	k_2 (g mg^{-1} min^{-1})	R^2
AFA	1.95 x 10^{-2}	0.6023	0.1315	0.9970
FA/Fe_3O_4	2.82 x 10^{-2}	0.6105	0.0328	0.9919

Based on the results given in **Table 2**, it can be seen that the adsorption process of MG dye on both AFA and FA/Fe_3O_4 adsorbents follows a pseudo-second-order kinetic model. The pseudo-first-order kinetic model shows very low R^2 values, e.g. 0.6023 for AFA and 0.6105 for FA/Fe_3O_4. On the other hand, the data evaluation using the pseudo second-order kinetic model gives the R^2 values of 0.99 which is very close to 1 for both AFA and FA/Fe_3O_4 adsorbents. Comparison of R^2 values between pseudo-first-order and pseudo-second-order kinetics leads to the conclusion that the adsorption of MG dye follows the pseudo-second-order kinetic model or the Ho and McKay kinetics model. Furthermore, the selection of this adsorption kinetic model is also supported by the theoretical q_e values, which closely approximate the experimental q_e values. The experimental q_e values are 3.691 mg/g for AFA and 8.538 mg/g for FA/Fe_3O_4, while the theoretical q_e values calculated from the pseudo-second-order kinetic model are 3.579 mg/g for AFA and 8.562 mg/g for FA/Fe_3O_4.

The pseudo-second-order adsorption kinetics indicates that the adsorption process consists of two stages an initial rapid stage followed by a slower second stage. The pseudo-second-order kinetic model in the adsorption process suggests the occurrence of chemical interactions. These interactions involve electrostatic interaction, hydrogen bonds or exchange or sharing of electrons between the adsorbent and adsorbate.

Effect of initial concentration of MG and isotherm adsorption studies

The results of the adsorption study about the effect of the initial concentration of MG dye on the adsorption capacity of AFA and FA/Fe_3O_4 adsorbents are presented in **Figure 8**. The adsorption capacity increases with the increasing initial concentration of MG dye until it reaches the optimal adsorption capacity at a certain initial concentration of the dye. This increase in adsorption capacity occurs because the active sites of the adsorbent that can interact with MG dye are still available in the adsorption system. Continuous interaction between the active sites of the adsorbent and the dye will continue to occur until the active sites of the adsorbent have been fully utilized and the system reaches the equilibrium state. Afterward, further increases in the initial concentration of the dye do not significantly affect the adsorption capacity, even in some cases the adsorption capacity experiences a slight decrease as observed in this study. This slight decline in capacity occurs possibly due to the continuing adsorption process with stirring after the equilibrium interaction between the adsorbent and the adsorbate has been attained, resulting in the desorption of some adsorbate that previously had been adsorbed. Another reason for the decrease in adsorption capacity is the diffusion issue. As the concentration of the adsorbate increases, the diffusion movement of the adsorbate in the solution towards the adsorption sites becomes more challenging, thereby reducing the amount of adsorbate adsorbed. The optimal initial concentration of MG dye that should be used in the adsorption process is 175 ppm for both AFA and FA/Fe_3O_4 adsorbents using 20 ml of solution and an adsorbent mass of 0.25 g for AFA and 0.1 g for FA/Fe_3O_4. The adsorption capacities obtained at the optimal initial concentration of MG are 7.61 mg/g for AFA and 17.37 mg/g for FA/Fe_3O_4 which is more than twice as high compared to that of AFA (see **Figure 9**). This higher adsorption capacity for FA/Fe_3O_4 is probably due to additional active sites originating from Fe_3O_4 surface, indicating that FA/Fe_3O_4 is more effective as an adsorbent for the cationic MG dye, besides it is also easily separable using an external magnet.

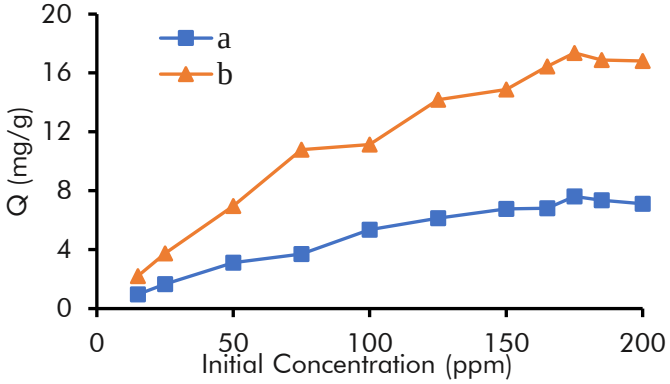

Figure 9. Effect of initial concentration on the adsorption of MG dye on AFA (**a**) and FA/Fe_3O_4 (**b**) adsorbents.

Table 3. Adsorption isotherm parameters for MG adsorption on AFA and FA/Fe_3O_4.

Isotherm parameters	AFA	FA/Fe_3O_4
Langmuir		
q_m (mg g^{-1})	8.24	21.59
K_L (L mol^{-1})	31683.67	15577.96
E_{ads} (kJ mol^{-1})*	25.68	23.92
R^2	0.9925	0.9841
Freundlich		
K_f (mg/g)	1.17	2.77
n	0.52	1.78
R^2	0.891	0.9238

*Adsorption energies E_{ads} (kJ mol^{-1}) were calculated based on Equation (6)

Table 4. Comparison of maximum adsorption capacity (q_m) of different types of adsorbents towards malachite green (MG) reported in the literature

Adsorbent Types	Maximum adsorption capacity (q_m, mg g^{-1})	References
Biomaterial of Arjun saal	53.19	Mandale, et al (2024)
Chitosan-ZnO composite	11.00	Muinde, et al (2020)
Nano-bentonite	13.80	Hussein Hamad (2023)
Mg-impregnated clay	17.20	
Alginate-Fe_3O_4 nanoparticles	47.80	Mohammadi, et al (2014)
Carbon active from wood apple shell	34.56	Sartape, et al (2017)
Activated coal fly ash (Muara Enim, Sumatra)	13.59	Nikmah, et al (2023)
AFA (PLTU, Cilacap)	8.24	This study
FA/Fe_3O_4	21.59	

The data obtained from the study of the effect of initial MG concentration are further used to determine the adsorption isotherm. The selection isotherm model suitable for the adsorption process is determined on the basis of the linearity value (R^2) of the plots using the corresponding equation of isotherm models. The isotherm model that exhibits an R^2 value closest to one is considered to be the most suitable isotherm model for this adsorption. In this study, two adsorption isotherm models have been used and the results of the adsorption isotherm evaluation using the two models are summarized in **Table 3.** From the table, it is observed that the adsorption process of MG dye on both AFA and FA/Fe_3O_4 adsorbents follows the Langmuir isotherm model, with R^2 values of 0.9925 and 0.9841, respectively. The Langmuir isotherm model assumes that the adsorption process occurs on a homogeneously active surface of the adsorbent, forms a monolayer adsorption mechanism, and involves the formation of chemical bonds between the adsorbent and the adsorbate (chemisorption). Based on the Langmuir adsorption isotherm model, the Langmuir constant (K_L), adsorption energy (E_{ads}), and the maximum adsorption capacity (q_m) at the equilibrium state can then be calculated and the results are given in **Table 3**.

The values of E_{ads} obtained for AFA and FA/Fe_3O_4 adsorbents are 25.68 and 23.92 kJ/mol, respectively. Adsorption can be considered to occur chemically when the E_{ads} values fall within the range of 20.9 to 418.4 kJ/mol (Adamson and Gast, 1997). The E_{ads} values for both AFA and FA/Fe_3O_4 adsorbents fall within this range, thus the adsorption of MG dye on AFA and FA/Fe_3O_4 adsorbents can be categorized as chemical adsorption, which is consistent with the result of the kinetic study. Again, we see here that the q_m values for FA/Fe_3O_4 adsorbents (21.59 mg/g) are almost three times higher than that of AFA (8.24 mg/g), indicating the efficiency of FA/Fe_3O_4 for the removal of MG dye. The adsorption capacity (q_m) of the developed adsorbents towards MG is also comparable with those of different adsorbents as depicted in **Table 4**.

CONCLUSIONS

The magnetized fly ash, FA/Fe_3O_4 adsorbent has been successfully synthesized from activated fly ash, AFA using the co-precipitation method, and the materials have been used for the adsorption of cationic malachite green dye, MG. The optimal conditions for the adsorption of MG dye are a solution pH of 7, an adsorbent mass of 0.25 g for AFA and 0.1 g for FA/Fe_3O_4, contact times of 45 minutes, and initial MG concentrations of 175 ppm. The MG adsorption process on both adsorbents follows a pseudo-second-order kinetic model and is best described by the Langmuir isotherm model. The adsorption capacity (q_m) for MG dye using FA/Fe_3O_4 adsorbents is almost

three times than using AFA, probably due to the additional active sites originating from ferrite, Fe_3O_4. The results demonstrate that magnetized FA/Fe_3O_4 adsorbent adsorbs cationic MG dye more efficiently than AFA and it can be a promising adsorbent for the removal of cationic MG in the waters because it is not only a more efficient adsorbent but also can be separated easily using external magnet after adsorption process.

ACKNOWLEDGMENTS

The partial financial support from DRTPM, DIKTI, Ministry of Education, Culture, Research and Technology, The Republic of Indonesia through Student Thesis Research (Penelitian Tesis Mahasiswa, PTM) scheme, decree number 0536/E5/PG.02.0012023 and contract number of I22IE5/PG.02.00.PL12023; 3223NNI/DITLIT/Dit-Lit/PT.01.0312023 is gratefully acknowledged.

REFERENCES

Ben, S. K., Gupta, S., Raj, K. K., & Chandra, V. (2023). Adsorption of malachite green from polyaniline facilitated cobalt phosphate nanocomposite from aqueous solution. *Chemical Physics Letters*, *820*(October 2022), 140469. https://doi.org/10.1016/j.cplett.2023.140469

Bharath Balji, G., Surya, A., Govindaraj, P., & Monisha Ponsakthi, G. (2022). Utilization of fly ash for the effective removal of hazardous dyes from textile effluent. *Inorganic Chemistry Communications*, *143*(February), 109708. https://doi.org/10.1016/j.inoche.2022.109708

Bojinova, D., & Teodosieva, R. (2016). Leaching of valuable elements from thermal power plant bottom ash using a thermo-hydrometallurgical process. *Waste Management and Research*, *34*(6), 511–517. https://doi.org/10.1177/0734242X16633775

Chowdhury, S., Mishra, R., Saha, P., & Kushwaha, P. (2011). Adsorption thermodynamics, kinetics and isosteric heat of adsorption of malachite green onto chemically modified rice husk. *Desalination*, *265*(1–3), 159–168. https://doi.org/10.1016/j.desal.2010.07.047

Du, B., Bai, Y., Pan, Z., Xu, J., Wang, Q., Wang, X., Lv, G., & Zhou, J. (2022). pH fractionated lignin for the preparation of lignin-based magnetic nanoparticles for the removal of methylene blue dye. *Separation and Purification Technology*, *295*(May), 121302. https://doi.org/10.1016/j.seppur.2022.121302

Harja, M., Buema, G., Lupu, N., Chiriac, H., Herea, D. D., & Ciobanu, G. (2021). Fly ash coated with magnetic materials: Improved adsorbent for cu (ii) removal from wastewater. *Materials*, *14*(1), 1–18. https://doi.org/10.3390/ma14010063

Huda, B. N. Wahyuni, E.T., Mudasir, M. (2023). Simultaneous adsorption of Pb(II) and Cd(II) in the presence of Mg(II) ion using eco-friendly immobilized dithizone on coal bottom ash. *South African Journal of Chemical Engineering*, *45*, 315–327. https://doi.org/10.1016/j.sajce.2023.06.007

Gracias, W., Huda, B.N., Suratman, A., Mudasir, M. (2022). Immobilization of dithizone on magnetic zeolite in less toxic medium and its application as adsorbent Cd(II) ion in water. *Materials Science Forum*, *1076*, 133–142. https://doi.org/10.4028/p-o0173e

Hussien Hamad, M.T.M. (2023). Optimization study of the adsorption of malachite green removal by MgO nano-composite, nano-bentonite and fungal immobilization on active carbon using response surface methodology and kinetic study. *Environmental Sciences Europe*, *35*, 26. https://doi.org/10.1186/s12302-023-00728-1

Islam, M. A., Ali, I., Karim, S. M. A., Hossain Firoz, M. S., Chowdhury, A. N., Morton, D. W., & Angove, M. J. (2019). Removal of dye from polluted water using novel nano manganese oxide-based materials. *Journal of Water Process Engineering*, *32*(August), 100911. https://doi.org/10.1016/j.jwpe.2019.100911

Jeyaseelan, C., Kaur, M., & Sen, M. (2023). Activated carbon modified chitosan beads: An effective method for removal of Congo Red dye. *Materials Today: Proceedings*, *xxxx*. https://doi.org/10.1016/j.matpr.2023.03.802

Jumaeri W, Astuti, & Lestari WTP. (2007). Preparasi dan Karakterisasi Zeolit Dari Abu Layang Batubara Secara Alkali Hidrotermal. In *Reaktor* (Vol. 11, Issue 1, pp. 38–44).

Kandisa, R. V., & Saibaba KV, N. (2016). Dye Removal by Adsorption: A Review. *Journal of Bioremediation & Biodegradation*, *07*(06). https://doi.org/10.4172/2155-6199.1000371

Karanac, M., Đolić, M., Veljović, Đ., Rajaković-Ognjanović, V., Veličković, Z., Pavićević, V., & Marinković, A. (2018). The removal of Zn2+, Pb2+, and As(V) ions by lime activated fly ash and valorization of the exhausted adsorbent. *Waste Management*, *78*, 366–378. https://doi.org/10.1016/j.wasman.2018.05.052

Kazemi, J., & Javanbakht, V. (2020). Alginate beads impregnated with magnetic Chitosan@Zeolite nanocomposite for cationic methylene blue dye removal from aqueous solution. *International Journal of Biological Macromolecules*, *154*, 1426–1437. https://doi.org/10.1016/j.ijbiomac.2019.11.024

Lee, A., Elam, J. W., & Darling, S. B. (2016). Membrane materials for water purification: Design, development, and application. *Environmental Science: Water Research and*

Technology, *2*(1), 17–42. https://doi.org/10.1039/c5ew00159e

Mandale, P., Kulkarni, K., Jadhav, K., Kulkarni, A., Mahajan, R. (2024). Adsorption of malachite green dye from aqueous solution on bioadsorbent as low-cost adsorbent. *Materials Today Proceeding*, In Press, Corrected Proof. https://doi.org/10.1016/j.matpr.2024.01.048

Mesdaghinia, A., Azari, A., Nodehi, R. N., Yaghmaeian, K., Bharti, A. K., Agarwal, S., Gupta, V. K., & Sharafi, K. (2017). Removal of phthalate esters (PAEs) by zeolite/Fe3O4: Investigation on the magnetic adsorption separation, catalytic degradation and toxicity bioassay. *Journal of Molecular Liquids*, *233,* 378–390. https://doi.org/10.1016/j.molliq.2017.02.094

Mohammadi, A., Daemi, H., Barikani, M. (2014). Fast removal of malachite green dye using novel superparamagnetic sodium alginate-coated Fe3O4 nanoparticles. *International Journal of Biological Macromolecules*. *69*, 447-455. https://doi.org/10.1016/j.ijbiomac.2014.05.042

Mohamed, A., Ghobara, M. M., Abdelmaksoud, M. K., & Mohamed, G. G. (2019). A novel and highly efficient photocatalytic degradation of malachite green dye via surface modified polyacrylonitrile nanofibers/biogenic silica composite nanofibers. *Separation and Purification Technology*, *210* (July 2018), 935–942. https://doi.org/10.1016/j.seppur.2018.09.014.

Muinde, V. M., Onyari, J. M., Wamalwa, B., Wabomba, J. N. (2020). Adsorption of malachite green dye from aqueous solutions using mesoporous chitosan–zinc oxide composite material. *Environmental Chemistry and Ecotoxicology*, *2*, 115-125. https://doi.org/10.1016/j.enceco.2020.07.005

Muttaqii, M. Al, Birawidha, D.C., Isnugroho, K., Amin, M., Hendronursito, Y., Istiqomah, A.D., and Dewangga, D.P., 2019, Pengaruh aktivasi secara kimia menggunakan larutan asam dan basa terhadap karakteristik zeolit alam, *Riset Teknologi Indonesia*, *13*, 266–271. https://doi.org/10. 26578/jrti.v13i2.5577

Nikmah, N., Roto, R., Mudasir, M. (2023). Isotherm and Kinetic Adsorption of Malachite Green Using Low-Cost Adsorbent of Coal Fly Ash. *Key Engineering Materials*, *949*, 163-173. https://doi.org/10.4028/p-08lw7P

Nourmoradi, H., Zabihollahi, S., & Pourzamani, H. R. (2016). Removal of a common textile dye, navy blue (NB), from aqueous solutions by combined process of coagulation–flocculation followed by adsorption. *Desalination and Water Treatment*, *57*(11), 5200–5211. https://doi.org/10.1080/19443994.2014.1003102

Saakshy, A., Singh, K., Gupta, A. B., & Sharma, A. K. (2016). Fly ash as low cost adsorbent for treatment of effluent of handmade paper industry-Kinetic and modelling studies for direct black dye. *Journal of Cleaner Production*, *112*, 1227–1240. https://doi.org/10.1016/j.jclepro.2015.09.058

Sartape, A. S., Mandhare, A. M., Jadhav, V. V., Raut, P. D., Anuse, M. A., & Kolekar, S. S. (2017). Removal of malachite green dye from aqueous solution with adsorption technique using Limonia acidissima (wood apple) shell as low cost adsorbent. *Arabian Journal of Chemistry*, *10*, S3229–S3238. https://doi.org/10.1016/j.arabjc.2013.12.019

Sulistiyo, Y. A., Rofi'ah, F., Suwardiyanto, Nugraha, A. S., Zulfikar, & Sunnardianto, G. K. (2020). Isothermal and kinetic adsorption of anionic dye onto impregnated silica gels with aluminum. *Environmental Engineering and Management Journal*, *19*(8), 1299–1308. https://doi.org/10.30638/eemj.2020.123

Susiana, C.A., Rusdiarso, B., Mudasir, M. (2024). Enhanced Capacity and Easily Separable Adsorbent of Dithizone-immobilized Magnetite Zeolite for Pb(II) Adsorption. *Indonesian Journal of Chemistry*, *24*(4), 1058–1070. https://doi.org/10.22146/ijc.90914

Suyanta, S., Falah, I.I., Nugroho, W., Fajariatri, K., Mudasir, M. (2022). Novel superparamagnetic nanocomposite of core-shell magnetic zeolite coated with chitosan crosslinked by glutaraldehyde: Synthesis and characterization. *Egyptian Journal of Chemistry*, *65*(3), 39–49. https://doi.org/10.21608/ejchem.2021.54439.3777

Umaningrum, D., Nurmasari, R., Santoso, U. T., Astuti, M. D., & Pradita, H. T. (2023). Adsorption of Congo Red onto Humic Acid Isolated from Peat Soil Gambut Regency, South Kalimantan. *Molekul*, *18*(2), 330. https://doi.org/10.20884/1.jm.2023.18.2.8685

Valeev, D., Mikhailova, A., & Atmadzhidi, A. (2018). Kinetics of iron extraction from coal fly ash by hydrochloric acid leaching. *Metals*, *8*(7), 1–9. https://doi.org/10.3390/met8070533

Yagub, M. T., Sen, T. K., Afroze, S., & Ang, H. M. (2014). Dye and its removal from aqueous solution by adsorption: A review. *Advances in Colloid and Interface Science*, *209*, 172–184. https://doi.org/10.1016/j.cis.2014.04.002

Zhang, Y., Chen, Y., Wang, C., & Wei, Y. (2014). Immobilization of 5-aminopyridine-2-tetrazole on cross-linked polystyrene for the preparation of a new adsorbent to remove heavy metal ions from aqueous solution. *Journal of Hazardous Materials*, *276*, 129–137. https://doi.org/10.1016/j.jhazmat.2014.05.027

Zhang, Y., Hui, C., Wei, R., Jiang, Y., Xu, L., Zhao, Y., Du, L., & Jiang, H. (2022). Study on anionic and cationic dye adsorption behavior and mechanism of biofilm produced by Bacillus amyloliquefaciens DT. *Applied Surface Science*, *573*(September 2021), 151627. https://doi.org/10.1016/j.apsusc.2021.151627